

## Electronic Supplementary Information for

# Direct $^{17}\text{O}$ NMR Experimental Evidence for Al-NBO Bonds in Si-Rich and Highly Polymerized Aluminosilicate Glasses

Aleksander Jaworski, Baltzar Stevansson, and Mattias Edén\*

Physical Chemistry Division, Department of Materials and Environmental Chemistry,  
Arrhenius Laboratory, Stockholm University, SE-106 91 Stockholm, Sweden

\*Corresponding author. E-mail: [mattias.eden@mmk.su.se](mailto:mattias.eden@mmk.su.se)

## Contents

1. **S1.** Materials and Methods
2. **Fig. S1.** Comparison between  $^{17}\text{O}$  NMR Spectra Recorded by Hard and Soft Rf Pulses
3. **Fig. S2.** Deconvoluted  $^{17}\text{O}$  MAS NMR Spectra
4. **Fig. S3.**  $^{17}\text{O}$  NMR Spectra Displayed over Expanded Ranges
5. **References**

## S1. Materials and Methods

### S1.1 Preparation of Si<sup>17</sup>O<sub>2</sub> and Al<sub>2</sub><sup>17</sup>O<sub>3</sub>

<sup>17</sup>O enriched H<sub>2</sub><sup>17</sup>O (36% <sup>17</sup>O; ISOTECH) was used to prepare the Si<sup>17</sup>O<sub>2</sub> and Al<sub>2</sub><sup>17</sup>O<sub>3</sub> precursors, each with an estimated enrichment degree of ≈30% <sup>17</sup>O. All synthesis stages were performed in Ar atmosphere.

Al<sub>2</sub><sup>17</sup>O<sub>3</sub> was obtained by dissolving aluminium isopropoxide, Al[OCH(CH<sub>3</sub>)<sub>2</sub>]<sub>3</sub>, in toluene. Small portions of H<sub>2</sub><sup>17</sup>O were then added while the temperature was controlled using an ice bath. The mixture was stirred constantly and refluxed for 2 h. The resulting xerogel was allowed to mature for 24 h and was subsequently heated at 1250 °C to yield the final α-Al<sub>2</sub><sup>17</sup>O<sub>3</sub> product.

Si<sup>17</sup>O<sub>2</sub> was prepared by dropwise addition of H<sub>2</sub><sup>17</sup>O to a solution of SiCl<sub>4</sub> in dried ether while stirring the mixture under flowing Ar to allow removal of HCl(g). The xerogel was dried at 100 °C under vacuum for 1.5 h. The final product of Si<sup>17</sup>O<sub>2</sub> was obtained after further heating at 500 °C.

### S1.2 Glass Synthesis and Characterization

RE AS glasses, simultaneously enriched in <sup>17</sup>O and <sup>29</sup>Si, were prepared in batches of 400 mg from high-purity oxide precursors of Lu<sub>2</sub>O<sub>3</sub>, Sc<sub>2</sub>O<sub>3</sub> and Y<sub>2</sub>O<sub>3</sub> from ChemPure (99.99% purity), and isotopically enriched materials of Al<sub>2</sub><sup>17</sup>O<sub>3</sub> (≈30% <sup>17</sup>O), Si<sup>17</sup>O<sub>2</sub> (≈30% <sup>17</sup>O), and <sup>29</sup>SiO<sub>2</sub> (96.7% <sup>29</sup>Si; EURISO-TOP). A mixture of 80% Si<sup>17</sup>O<sub>2</sub> and 20% <sup>29</sup>SiO<sub>2</sub> was used as a source for Si to ensure ≈20% <sup>29</sup>Si enrichment of all glasses. Each oxide was first calcined at 600 °C for 3 hours (300 °C for the isotopically labeled materials) to remove the potential presence of hydroxyl and/or carbonate impurities. The precursors were weighted in appropriate amounts to match each RE AS composition listed in Table 1. They were next mixed in a mortar for 1 h. Except for the Lu AS glasses, each batch also incorporated paramagnetic doping by 0.05–0.1 wt% Gd<sub>2</sub>O<sub>3</sub> to enhance <sup>17</sup>O spin-lattice relaxation for the NMR experimentation.

Each oxide mixture was heated in a Pt crucible in an electric furnace under Ar atmosphere at 1600 °C (Y-based glasses) or 1650 °C (Lu and Sc bearing glasses). The melt was quenched by immersing the bottom of the crucible in water. The weight losses during synthesis remained consistently below 2.0%.

Owing to the substantial costs of the isotopically enriched precursors, no invasive characterizations were employed, but the integrity of the compositions of the resulting glasses were verified by their essentially identical <sup>27</sup>Al and <sup>29</sup>Si NMR spectra observed relative to those collected from specimens prepared simultaneously as the (<sup>17</sup>O, <sup>29</sup>Si) enriched samples but using precursors with each element at its natural abundance level. The monophasic amorphous character of the latter glasses were confirmed by powder X-ray diffraction and scanning electron microscopy (SEM) in backscatter mode (JSM 7000F, JEOL). SEM coupled with energy-dispersive X-ray spectroscopy (EDS) verified that each composition was very close (typically within ±(0.5–1.0) at%) to its batched counterpart listed in Table 1. We refer to our previous reports for further details on RE AS glass synthesis and characterizations.<sup>S1–S5</sup>

### S1.3 Solid-State NMR Experimentation

MAS NMR experiments were carried out on Bruker Avance-III spectrometers at the magnetic fields of  $B_0=9.4$  T (<sup>17</sup>O Larmor frequency  $\nu_0=54.3$  MHz) and  $B_0=14.1$  T ( $\nu_0=81.4$  MHz). 4 mm triple resonance (TR) MAS probeheads were used at both fields, with the experimentation at 14.1 T additionally involving a 3.2 mm TR MAS probehead. Finely ground samples were packed into zirconia rotors and spun at the MAS rates of  $\nu_r=24.000$  kHz and  $\nu_r=14.000$  kHz for the

experimentation with the 3.2 mm and 4.0 mm probeheads, respectively. For each experimental condition, the MAS rate is sufficiently high to move all spinning sidebands outside of the spectral region of the centerband CT signals; see Fig. **S3** that reproduces the spectra of Fig. **1** over an expanded spectral window.  $^{17}\text{O}$  and  $^{27}\text{Al}$  chemical shifts are quoted relative to water and a 1 M  $\text{Al}(\text{NO}_3)_3(\text{aq})$  solution, respectively; these liquids were also utilized for estimating radio-frequency (rf) nutation frequencies.

$^{17}\text{O}$  MAS NMR spectra were collected by using central transition (CT) selective pulses operating at a nutation frequency of  $\nu_{\text{O}}^{\text{CT}}=18.0$  kHz, corresponding to a  $90^\circ$  pulse length of  $14.0 \mu\text{s}$ . The relaxation delays ranged between 30–45 s and were determined for each individual sample from separately recorded  $T_1$  measurements to ensure quantitative results. 5120–7168 signal transients were accumulated for experiments performed at 14.1 T (3.2 mm probehead), whereas those acquired at 9.4 T (4 mm probehead) employed 1600–2240 transients.

The  $^{17}\text{O}\{^{27}\text{Al}\}$  TRAPDOR<sup>S6</sup> NMR experiments involved an  $^{17}\text{O}$  spin-echo of total duration  $2\tau_{\text{rec}}$ , with a CT-selective  $^{17}\text{O}$   $180^\circ$  pulse of  $28.4 \mu\text{s}$ . A high-power ( $\nu_{\text{Al}}=74.0$  kHz) recoupling pulse of duration  $\tau_{\text{rec}}=2.5$  ms was applied to  $^{27}\text{Al}$  for arranging the dipolar-dephased NMR signal  $S(\tau_{\text{rec}})$ , whereas the “reference” experiment  $S_0(\tau_{\text{rec}})$  was performed in the absence of  $^{27}\text{Al}$  radio-frequency irradiation. 7168–11264 signal transients were accumulated.

Ramped<sup>S7</sup>  $^{27}\text{Al}\rightarrow^{17}\text{O}$  RAPT-CP<sup>S8</sup> experiments were performed at 14.1 T and 14.0 kHz MAS with a 5.0 ms contact interval and matched radio-frequency fields of  $\nu_{\text{Al}}^{\text{CT}}=22.0$  kHz and  $\nu_{\text{O}}^{\text{CT}}=8.0$  kHz for  $^{27}\text{Al}$  and  $^{17}\text{O}$ , respectively. This obeys the modified Hartmann-Hahn condition  $\nu_{\text{Al}}^{\text{CT}}=\nu_{\text{O}}^{\text{CT}}+\nu_r$ . Each NMR acquisition involved 36864–50176 accumulated transients.

Saturation-recovery blocks were used prior to relaxation delays of 5.0 s and 2.5 s for all TRAPDOR and RAPT-CP NMR experiments, respectively. All double resonance experiments involved the RAPT<sup>S9</sup> technique for CT-signal enhancement. Roughly 30 RAPT blocks were used with equal durations of the pulses and delays of  $0.95 \mu\text{s}$  for  $^{17}\text{O}$  (TRAPDOR) and  $0.70 \mu\text{s}$  for  $^{27}\text{Al}$  (RAPT-CP), in both cases using a nutation frequency of 74.0 kHz.

## S1.4 NMR Spectra Deconvolutions

By using in-house developed software based on numerically exact spin-dynamics simulations that account for all time-dependent interactions and experimental parameters (see Refs. S3 and S5 and references therein for further details), the CT-signal region of each  $^{17}\text{O}$  MAS NMR spectrum of Fig. **1** was deconvoluted into component peaks from two NBO moieties ( $\text{Al-O}^{[1]}$ ,  $\text{Si-O}^{[1]}$ ), and three BO contributions ( $\text{Al-O}^{[2]}-\text{Al}$ ,  $\text{Al-O}^{[2]}-\text{Si}$ ,  $\text{Si-O}^{[2]}-\text{Si}$ ). The various NBO and BO populations will be discussed in detail for an extensive set of RE AS glasses in a forthcoming publication. Here we focus on the *total* fractional populations of each BO ( $x^{[2]}$ ) and NBO ( $x^{[1]}$ ) speciation, and the contributions to the NBO speciation from each  $\text{Si-O}^{[1]}$  ( $x_{\text{Si}}^{[1]}$ ) and  $\text{Al-O}^{[1]}$  ( $x_{\text{Al}}^{[1]}$ ) bonding scenario, i.e., the  $^{17}\text{O}$  NMR-derived  $\{x^{[1]}, x_{\text{Si}}^{[1]}, x_{\text{Al}}^{[1]}\}$  values listed in Table **1**.

Besides the various fractional populations, the numerical fitting accounted for the *average* isotropic chemical shift ( $\bar{\delta}_{\text{iso}}$ ) and quadrupolar product  $\bar{C}_{Q\eta}=\bar{C}_Q(1+\eta^2/3)^{1/2}$  of each BO/NBO species, where  $\bar{C}_Q$  and  $\eta$  denote the quadrupolar coupling constant and asymmetry parameter of the electric field gradient tensor, respectively.<sup>S10,S11</sup> Czjzek<sup>S12</sup> and Gaussian (with  $W_{\text{iso}}$  denoting the FWHM in ppm) distributions were assumed for the quadrupolar products and  $^{17}\text{O}$  isotropic chemical shifts, respectively. For each of the five peak components, both values of  $\bar{\delta}_{\text{iso}}$  and  $W_{\text{iso}}$  were restricted within  $\pm 4$  ppm. Figure **S2** shows two examples of deconvolution results. To better constrain the numerical fitting,  $^{17}\text{O}$  MAS NMR spectra recorded at  $B_0=9.4$  T (not shown) by using short and strong pulses were fitted simultaneously with those acquired at  $B_0=14.1$  T by CT-selective pulses (i.e., those presented in Fig. **1**). Note that the latter  $^{17}\text{O}$  NMR spectra agreed

very well with results obtained by “hard” pulses under otherwise identical experimental conditions, as illustrated by Fig. S1.

## S1.5 Molecular Dynamics Simulations

Each glass model was obtained by an atomistic MD simulation that emulated the melt-quench procedure for an NVT ensemble in a cubic box with periodic boundary conditions.<sup>S13</sup> The calculations were performed with the DLPOLY3 package,<sup>S14,S15</sup> using 3000–9000 atoms. The box-length was adjusted to match the experimental density and composition of each RE AS glass, using our previously reported densities for glasses involving Y,<sup>S3</sup> Lu,<sup>S3</sup> and Sc.<sup>S5</sup>

The melt-quench simulation started from a structure equilibrated at 3500 K for 100 ps, followed by a 10 ps step-wise decrease of 10 K/ps down to 300 K, where equilibration was performed during 200 ps, of which the trajectory during the last 150 ps was used for the structural analysis. For each glass composition, this protocol was completed 4–8 times with distinct initial atom configurations, each generated by a random distribution subject to the constraint of a 50 pm minimum distance in any atom-pair. The average value and uncertainty of each modeled structural parameter was derived from these distinct trajectories: the populations of the various  $O^{[p]}$  ( $p = 0, 1, 2, 3$ ) listed in Table 1 were obtained by integrating the  $g_{O-E}(r)$  pair distribution function ( $E = \{\text{Si}, \text{Al}\}$ ) out to 250 pm.

The interatomic potentials included both long-range Coulombic and short-range Buckingham (or Born-Mayer) terms: the precise parameters are provided in Table 1 of Okhotnikov *et al.*<sup>S16</sup> that also describes the procedures for obtaining and validating each RE–O potential parameter. Partial charges of  $-1.2e$  for O,  $2.4e$  for Si, and  $1.8e$  for Al as well as all RE species were employed,<sup>S17</sup> where  $e$  is the elementary charge. A modified Buckingham potential<sup>S18</sup> was implemented to circumvent strong attractions at small interatomic distances; it was evaluated for all atom-pairs out to 0.8 nm, whereas the Coulombic interactions were calculated by a smoothed particle mesh Ewald summation<sup>S15</sup> with a 1.2 nm real-space cut-off and an accuracy of  $10^{-6}$ . The equations of motion were integrated in time-steps of 2 fs by the velocity Verlet integrator approach, whereas the temperature was controlled by a Berendsen thermostat with a 1.0 ps relaxation time constant.<sup>S13</sup>

For additional information about the MD simulation procedures, we refer the reader to our previous reports and results for RE AS glasses.<sup>S3,S16</sup>

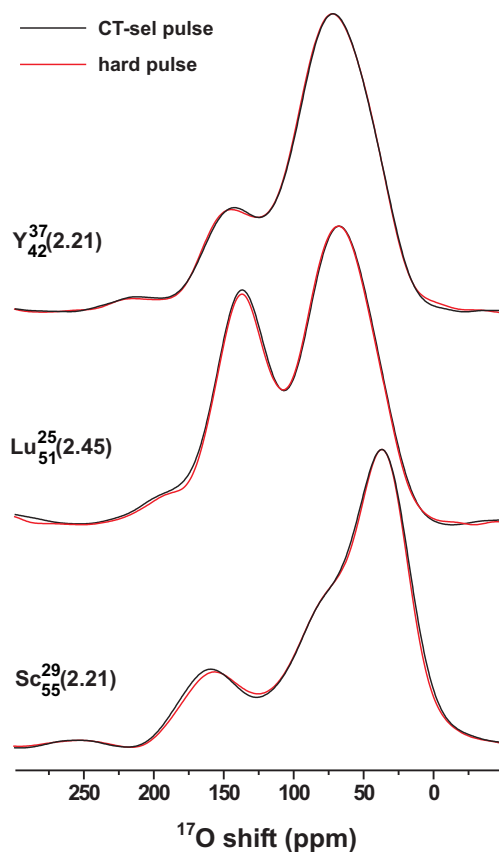


**Fig. S1.** A selection of  $^{17}\text{O}$  MAS NMR spectra recorded at  $B_0 = 14.1$  T and 24.00 kHz MAS from the as-indicated AS glasses. The results were recorded either by CT-selective  $90^\circ$  pulses (black traces; spectra reproduced from Fig. 1) or by short ( $0.25 \mu\text{s}$ ), strong ( $\nu_{\text{O}}=74.0$  kHz) pulses (red traces), the latter corresponding to a flip angle of  $6.7^\circ$ . Note the excellent agreement between the two results of the distinct excitation conditions. This confirms the quantitative character of the spectra obtained by the CT-selective pulses (Fig. 1) that were used to derive the various  $\{\text{O}^{[1]}, \text{O}^{[2]}\}$  populations of Table 1.

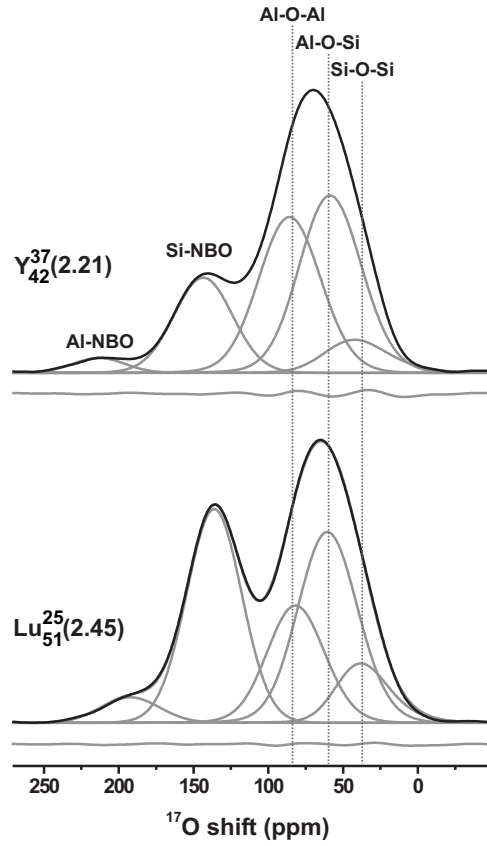


**Fig. S2.** Experimental  $^{17}\text{O}$  MAS NMR spectra (black traces) recorded by CT-selective pulses from the (a)  $\text{Y}_{42}^{37}(2.21)$  and (b)  $\text{Lu}_{51}^{25}(2.45)$  glasses at  $B_0=14.1$  T and  $\nu_r=24.00$  kHz. The spectra are shown together with deconvolution results into five component peaks constituting two  $^{17}\text{O}^{[1]}$  resonances (Al-NBO, Si-NBO) and three  $\text{O}^{[2]}$  signals (Al-O-Al, Al-O-Si, Si-O-Si). The curve beneath each NMR spectrum represents the difference between the experimental and best-fit spectra.

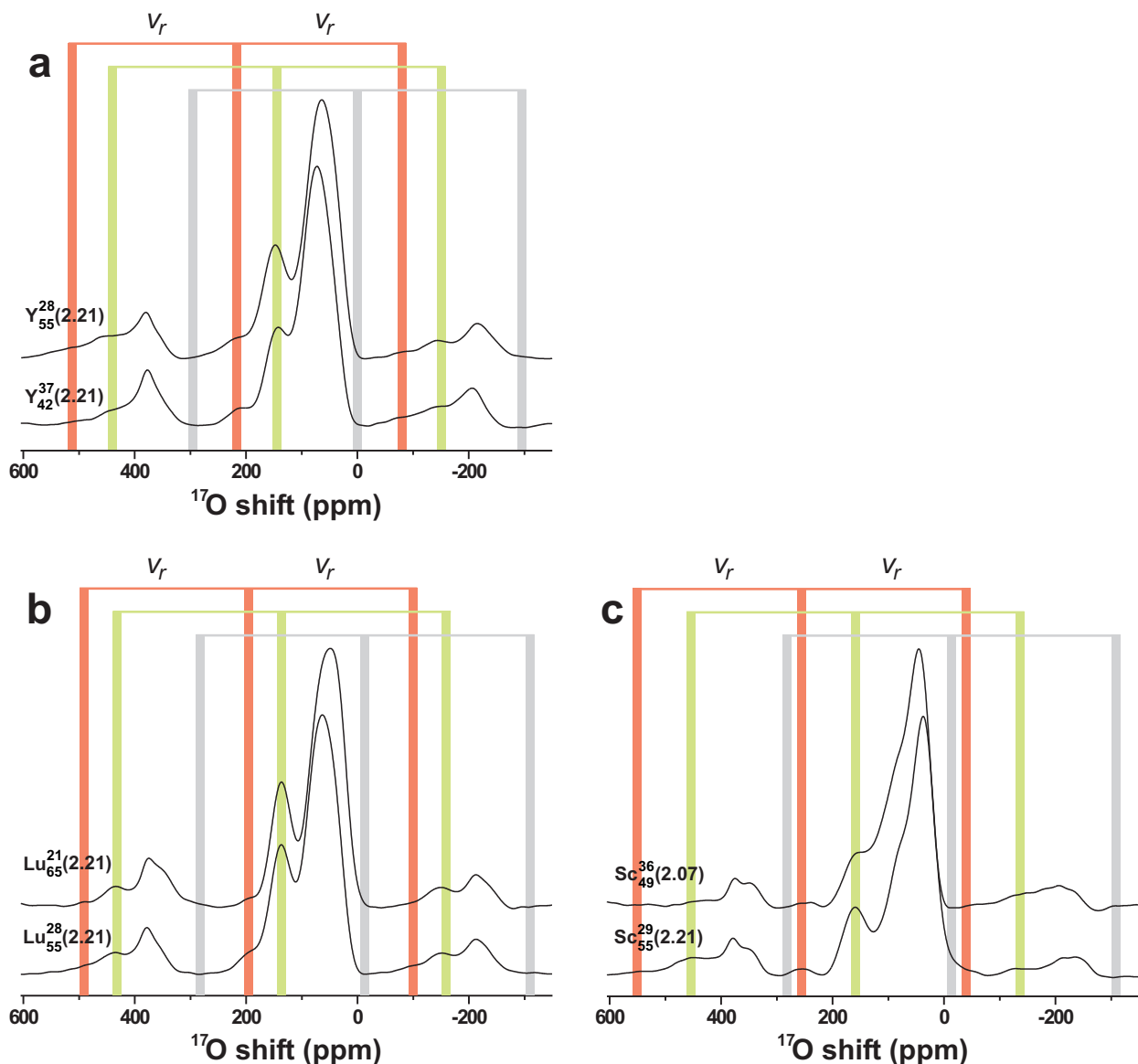


**Fig. S3.** The  $^{17}\text{O}$  MAS NMR spectra of Fig. 1 ( $B_0=14.1$  T;  $\nu_r=24.00$  kHz) for the as-indicated (a) Y, (b) Lu, and (c) Sc glasses, displayed over an expanded ppm-range that also includes the first-order spinning sidebands. Each *center* green and red narrow rectangle marks the centerband position of the  $^{17}\text{O}$  peak assigned to Al-NBO and Si-NBO fragments, respectively; the corresponding left/right rectangles indicate the ppm-coordinates within the sidebands that are shifted from the centerband position by  $\pm\nu_r$  (i.e., by  $\pm 24.00$  kHz;  $\pm 295.0$  ppm). The respective set of three grey rectangles is centered at the *lowest* shift of the  $^{17}\text{O}^{[2]}$  centerband signal: hence, the left-most grey rectangle mark the *highest* ppm-value at which the first-order sideband of the BO resonance could appear. Notably, the MAS rate is sufficiently large to move all sidebands outside of the CT-centerband region, particularly in the case of the NMR spectra recorded from the Y and Lu glasses in (a, b). Roughly the same relative positioning of the center/side-bands applies for the TRAPDOR NMR spectra in Fig. 2, which were obtained at  $B_0=9.4$  T and  $\nu_r=14.00$  kHz. Note that while the NMR peak from the Al-NBO groups of the Sc-bearing glasses in (c) is unambiguously present as a unique resonance, it may carry a minor sideband component beneath the right-most portion of the  $^{17}\text{O}^{[2]}$  centerband (whose integrated intensity is automatically accounted for by the numerical simulations used in the spectra deconvolution).

## References

- (S1) S. Iftekhhar, J. Grins, and M. Edén, Composition-property relationships of the  $\text{La}_2\text{O}_3\text{-Al}_2\text{O}_3\text{-SiO}_2$  glass system, *J. Non-Cryst. Solids*, 2010, **356**, 1043–1048.
- (S2) S. Iftekhhar, J. Grins, P. N. Gunawidjaja, and M. Edén, Glass formation and structure-property-composition relations of the  $\text{RE}_2\text{O}_3\text{-Al}_2\text{O}_3\text{-SiO}_2$  (RE=La, Y, Lu, Sc) systems, *J. Am. Ceram. Soc.*, 2011, **94**, 2429–2435.
- (S3) S. Iftekhhar, B. Pahari, K. Okhotnikov, A. Jaworski, B. Stevansson, J. Grins, and M. Edén, Properties and structures of  $\text{RE}_2\text{O}_3\text{-Al}_2\text{O}_3\text{-SiO}_2$  (RE=Y, Lu) glasses probed by molecular dynamics simulations and solid-state NMR: The roles of aluminum and rare-earth ions for dictating the microhardness, *J. Phys. Chem. C*, 2012, **116**, 18394–18406.
- (S4) A. Jaworski, B. Stevansson, B. Pahari, K. Okhotnikov, and M. Edén, Local structures and Al/Si ordering in lanthanum aluminosilicate glasses explored by advanced  $^{27}\text{Al}$  NMR experiments and molecular dynamics simulations, *Phys. Chem. Chem. Phys.*, 2012, **14**, 15866–15878.
- (S5) B. Pahari, S. Iftekhhar, A. Jaworski, K. Okhotnikov, K. Jansson, B. Stevansson, J. Grins, and M. Edén, Composition-property-structure correlations of scandium aluminosilicate glasses revealed by multinuclear  $^{45}\text{Sc}$ ,  $^{27}\text{Al}$  and  $^{29}\text{Si}$  solid state NMR, *J. Am. Ceram. Soc.*, 2012, **95**, 2545–2553.
- (S6) C. P. Grey and W. S. Veeman, The detection of weak heteronuclear coupling between spin 1 and spin 1/2 nuclei in MAS NMR;  $^{14}\text{N}/^{13}\text{C}/^1\text{H}$  triple resonance experiments, *Chem. Phys. Lett.*, 1992, **192**, 379–385.
- (S7) G. Metz, X. Wu, and S. O. Smith, Ramped-amplitude cross polarization in magic-angle-spinning NMR, *J. Magn. Reson. Ser. A*, 1994, **110**, 219–227.
- (S8) M. Edén, J. Grins, Z. Shen, and Z. Weng, Fast  $^{29}\text{Si}$  magic-angle-spinning NMR acquisitions by  $^{27}\text{Al}\rightarrow^{29}\text{Si}$  RAPT-CP polarization transfer, *J. Magn. Reson.*, 2004, **169**, 279–283.
- (S9) Z. Yao, H.-T. Kwak, D. Sakellariou, L. Emsley, and P. J. Grandinetti, Sensitivity enhancement of the central transition NMR signal of quadrupolar nuclei under magic-angle spinning, *Chem. Phys. Lett.*, 2000, **327**, 85–90.
- (S10) M. Edén, Computer simulations in solid state NMR: I. Spin dynamics theory, *Concepts Magn. Reson. A*, 2003, **17**, 117–154.
- (S11) M. Edén, NMR Studies on oxide-based glasses, *Annu. Rep. Prog. Chem., Sect. C: Phys. Chem.*, 2012, **108**, 177–221.
- (S12) G. Czjzek, J. Fink, F. Götz, H. Schmidt, J. M. D. Coey, J.-P. Rebouillat, and A. Liénard, Atomic coordination and the distribution of electric field gradients in amorphous solids, *Phys. Rev. B.*, 1981, **23**, 2513–2530.
- (S13) M. P. Allen and D. J. Tildesley, *Computer Simulation of Liquids*, Oxford, Clarendon, 1989.
- (S14) W. Smith and T. R. Forester, DL\_POLY\_2.0: A general-purpose parallel molecular dynamics simulation package, *J. Mol. Graphics*, 1996, **14**, 136–141.

- (S15) I. T. Todorov, W. Smith, K. Trachenko, and M. T. Dove, DL\_POLY\_3: New dimensions in molecular dynamics simulations via massive parallelism, *J. Mater. Chem.*, 2006, **16**, 1911–1918.
- (S16) K. Okhotnikov, B. Stevansson, and M. Edén, New interatomic potential parameters for molecular dynamics simulations of rare-earth (RE=La, Y, Lu, Sc) aluminosilicate glass structures: Exploration of RE<sup>3+</sup> field-strength effects, *Phys. Chem. Chem. Phys.*, 2013, **15**, 15041–15055.
- (S17) B. W. H. van Beest, H. J. Kramer, and R. A. van Santen, Force fields for silicas and aluminophosphates based on *ab initio* calculations, *Phys. Rev. Lett.*, 1990, **64**, 1955–1958.
- (S18) V. A. Bakaev and W. A. Steele, On the computer simulation of a hydrophobic vitreous silica surface, *J. Chem. Phys.*, 1999, **111**, 9803–9812.